Supramolecular host-guest chemistry for applications in theranostics
Spa, S.J.

Citation
Spa, S. J. (2019, May 9). *Supramolecular host-guest chemistry for applications in theranostics.*
Retrieved from https://hdl.handle.net/1887/72514

Version:	Not Applicable (or Unknown)
License:	[Leiden University Non-exclusive license](https://hdl.handle.net/1887/72514)
Downloaded from:	https://hdl.handle.net/1887/72514

Note: To cite this publication please use the final published version (if applicable).

Cover Page

Universiteit Leiden

The handle http://hdl.handle.net/1887/72514 holds various files of this Leiden University dissertation.

Author: Spa, S.J.
Title: Supramolecular host-guest chemistry for applications in theranostics
Issue Date: 2019-05-09

CHAPTER **4**

In vivo stability of supramolecular host–guest
complexes monitored by dual–isotope
multiplexing in a pre–targeting model of
experimental liver radioembolization

ABSTRACT

Introduction

Cyclodextrin (CD) based supramolecular interactions have been proposed as nanocarriers for drug delivery. We previously explored the use of supramolecular interactions to perform targeted hepatic radioembolization. In a two-step procedure the appropriate location of the diagnostic pre-targeting vector can first be confirmed, after which the therapeutic vector will be targeted through multivalent host-guest interactions. Such a procedure would prevent therapeutic errors due to a mismatch between diagnostic and therapeutic procedures. In the current study we explored the use of dual-isotope imaging to assess the in vivo stability of the formed complex and individual components.

Methods

Dual-isotope imaging of the host and guest vectors was performed after labeling of the pre-targeted guest vector, being adamantane (Ad) functionalized macro-aggregated albumin (MAA) particles, with technetium-99m (^{99m}Tc-MAA-Ad). The host vector, Cy5$_{0.5}$CD$_9$PIBMA$_{39}$, was labeled with indium-111 (^{111}In-Cy5$_{0.5}$CD$_9$PIBMA$_{39}$). The *in situ* stability of both the individual vectors and the resulting [MAA-Ad–^{111}In-Cy5$_{0.5}$CD$_9$PIBMA$_{39}$] complexes was studied over 44 h at 37 °C in a serum protein-containing buffer. *In vivo*, the host vector ^{111}In-Cy5$_{0.5}$CD$_9$PIBMA$_{39}$ was administered two hours after local deposition of ^{99m}Tc-MAA-Ad in mice. Dual-isotope SPECT imaging and quantitative biodistribution studies were performed at 2 and until 44 h post intravenous host vector administration.

Results

The individual vectors portrayed less than 5% dissociation of the radioisotope over the course of 20 h. Dissociation of [MAA-Ad–^{111}In-Cy5$_{0.5}$CD$_9$PIBMA$_{39}$] complexes remained within a 10–20% range after incubation in serum. *In vivo* dual-isotope SPECT imaging of host–guest interactions revealed co-localization of the tracer components. Quantitative assessment of the biodistribution revealed that the hepatic accumulation of the host vector nearly doubled between 2 h and 44 h post-injection (from 14.9 ± 6.1 %ID/g to 26.2 ± 2.1 %ID/g).
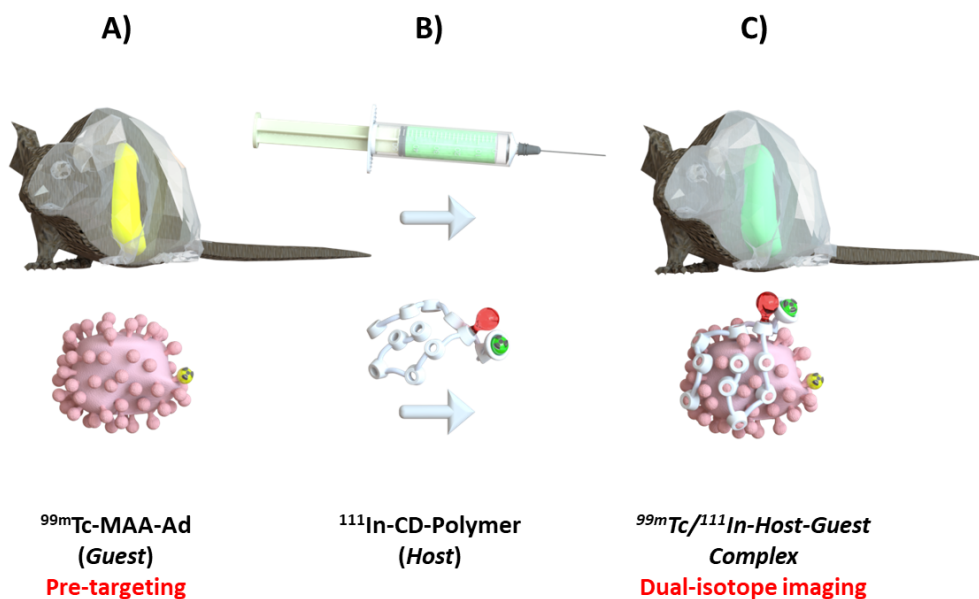
Conclusions

Assessment of intra-hepatic host–guest complexation was successfully achieved using dual isotope multiplexing, underlining the complex stability that was found in situ (up to 44 h in serum). Overall, the results obtained in this study highlight the potential of supramolecular chemistry as a versatile platform that could advance the field of nanomedicine.

INTRODUCTION

Hepatocellular carcinoma (HCC) and liver metastases of colorectal cancer (mCRC) are the third most common cause of cancer-related deaths worldwide.[1,2] With currently 1.12 million deaths worldwide per year, both the incidence of these cancer types and their impact on health expenditure is increasing. Surgical excision is considered the fist-line therapy but cannot be applied in grade 3–5 staged HCC. The substantial portion of inoperable patients that present metastatic liver tumors are therefore in need of alternative treatment strategies[3-5] One relatively novel treatment option that has presented potential to effectively manage these hepatic tumors is radio- or chemo-embolization[6]; of these two radioembolization is the most frequently applied. In HCG patients this embolization strategy has proven to be beneficial to survival in patients with HCG.[7]

Radioembolization is performed using a two-step interventional radiological theranostic procedure. In this procedure Single Positron Emission Computed Tomography (SPECT) imaging of macro-aggregated albumin (scout scan delivered by a CT guided catheter; ^{99m}Tc-MAA; d = 10–40 μm) is used to explore the potential of selective internal radiotherapy (i.e., radioembolization). When correct localization of the ^{99m}Tc-MAA is visualized, therapeutic β-emitting microparticles (d = 15–25 μm)[8] containing ^{90}Y (SIR-Spheres®, Sirtex; Therasphere, BTG®) or ^{166}Ho (QuiremSpheres; Quirem Medical) are injected two weeks later via the same positioned catheter in the *a. hepatica*.[9] The overlap in size and retention properties between the albumin macroaggregates and the microparticles has been sufficient for the clinical guidelines to define a ^{99m}Tc-MAA scout scan as a standard requirement to predict accurate delivery of therapeutic microspheres during a second intervention. Despite this inclusion in the guidelines, a mismatch between the scout scan and therapy delivery which can lead to adverse side effects and suboptimal dose delivery[6] is seen in 30% of the cases.[10-12] This indication signifies a need for innovative solutions that help refine the correlation between the two interventions (*i.e.*, the scout scan and therapeutic delivery). Another drawback is the delay (≈ 14 days) between the execution of the scout scan and the therapeutic intervention that mainly occurs as result of the production/delivery time of the β-emitting microspheres.[9]

While some groups have proposed to use low-dose application of therapeutic microspheres during scout scans,[13] we have previously explored an alternative route based on the use of a pre-targeting strategy. In this latter approach, the agent used to create a diagnostic scout scan provides the target for a secondary agent containing the therapeutic component. As proof of concept we explored cyclodextrin (CD)-based host and adamantane

A)   **B)**   **C)**

^{99m}Tc-MAA-Ad   **^{111}In-CD-Polymer**   **^{99m}Tc/^{111}In-Host-Guest**
(*Guest*)   **(*Host*)**   **Complex**
Pre-targeting   **Dual-isotope imaging**

Scheme 1. Representation of the pre-targeting radioembolization concept: **A)** Firstly, ^{99m}Tc-MAA-Ad was administered into the liver of a mouse. **B)** After 2 h, an ^{111}In- Cy5$_{0.5}$CD$_9$PIBMA$_{39}$ was intravenously administered. **C)** Dual-isotope imaging was performed to assess the co-localization of both compounds at various intervals until 44 h p.i. **Legend:** adamantane (Ad; guest), ^{99m}Tc-labeled and Ad-functionalized macro-aggregated albumin (^{99m}Tc-MAA-Ad; guest vector), cyclodextrin (CD), cyclodextrin functionalized poly(isobutylene-*alt*-maleic-anhydride polymer (Cy5$_{0.5}$CD$_9$PIBMA$_{39}$, host vector), ^{111}In- Cy5$_{0.5}$CD$_9$PIBMA$_{39}$ (radiolabeled host vector).

(Ad) guest interactions on a MAA platform.[14] When functionalized with Ad guest-moieties (yielding MAA-Ad; guest vector), the compound used for the diagnostic scout scan, could be used as the target for a secondary CD-containing host vector, which is in this case was a ^{99m}Tc-labeled CD-functionalized Poly(isobutylene-*alt*-maleic-anhydride) polymer (^{99m}Tc-Cy5$_n$CD$_n$PIBMA$_{n''}$). The encouraging *in vivo* data obtained with this set-up indicated that supramolecular host–guest interactions could provide an alternative means for radioembolization procedures.[15]

In the study presented here we expand our previous efforts by studying the stability of the host–guest complexes over a period that matches the timespan of the clinical radioembolization procedure. Dual-isotope SPECT imaging (see Scheme 1) was used to individually track both the host (CD-functionalized polymer labeled with Cy5 and ^{111}In ($t_{1/2}$ = 2.9 d, 170 & 240 KeV)) and guest (MAA-Ad radiolabeled with ^{99m}Tc ($t_{1/2}$ = 6 h, 140 KeV))

vector.[16] To evaluate the integrity of the individual compounds and the host–guest complexes formed, *in vitro* and *in vivo* stability studies were related to *in vivo* SPECT imaging and quantitative biodistribution patterns of both components. These longitudinal assessments were then used to determine the chemical refinements that are required to contemplate translation of the technology into the clinic.

Materials and Methods

General analytical procedures and information on the materials used are provided in the Supporting Information (SI).

Synthesis and analysis

Synthesis and characterization of both adamantane-tetrafluorophenol (Ad-TFP) and β-cyclodextrin-poly(isobutylene-alt-maleic-anhydride) ($Cy5_{0.5}CD_9PIBMA_{39}$, ~18.7 kDa, diameter, ~11.7 nm) were carried out as recently described in.[14, 15]

Radiolabeling of host vector MAA(-Ad) with technetium-99m and stability testing

Labeling of macro-aggregated albumin (MAA) with technetium (^{99m}Tc-MAA) and functionalization with Ad-TFP was carried out as described previously.[15] The stability of the ^{99m}Tc-chelation was determined in fetal calf serum (FCS, Life Technologies Inc. CA) after 2, 4, and 20 h. The release of radioactivity was determined after centrifugation and two washing steps with PBS (3 min, 1,200xg) as described previously.[15]

Labeling of $Cy5_{0.5}CD_9PIBMA_{39}$ with indium-111 (^{111}In-$Cy5_{0.5}CD_9PIBMA_{39}$) and stability testing

The host-vector, $Cy5_{0.5}CD_9PIBMA_{39}$, which contains an abundance of freely available -COOH moieties, was radiolabeled with indium-111. To 10 μL of $Cy5_{0.5}CD_9PIBMA_{39}$ (1 mg/mL PBS) was added 40 mL of 0.25 M ammonium acetate (pH 5) and 25-150 mL of an acidic solution of $^{111}InCl_3$ (370 MBq/mL, Mallinckrodt Medical, Petten, The Netherlands). This mixture was gently shaken in the dark for 1 h at 37 °C. Thereafter, the pH was adjusted to 7.5 in PBS. The radiochemical purity of ^{111}In-$Cy5_{0.5}CD_9PIBMA_{39}$ was determined at 1 and 20 h by instant thin layer chromatography (ITLC) on 1x7 cm ITLC-SG paper strips (Agilent Technologies, USA) with 0.25 M ammonium acetate (pH 5) as mobile phase.

The serum stability of the ^{99m}Tc-chelation was determined in fetal calf serum (FCS, Life Technologies Inc. CA). After 24 h the release of radioactivity was determined with centrifugation and washing steps as described above. To determine the stability in FCS,

^{111}In-Cy$_{0.5}$CD$_9$PIBMA$_{39}$ was diluted in FCS (2.5 µg/mL) and shaken in a water bath at 37 °C for 20 h. After 2, 4, and 20 h samples of 0.1 mL were taken and the release of radioactivity was assessed by ITLC. For comparison, a similar set-up was performed for ^{111}In-Cy$_{0.5}$CD$_9$PIBMA$_{39}$.[15]

In vitro host-guest interactions and complex stability

In line with previous studies,[15] *in vitro* evidence for the host-guest complex formation between MAA-Ad and ^{111}In-Cy$_{0.5}$CD$_9$PIBMA$_{39}$ was provided by comparing the ^{111}In-Cy$_{0.5}$CD$_9$PIBMA$_{39}$ binding to MAA-Ad and non-functionalized MAA (control). Mixtures of 0.1 mL containing either MAA-Ad or MAA (0.1 mg/mL) with 0.1 mL ^{111}In-Cy$_{0.5}$CD$_9$PIBMA$_{39}$ (10 µg/mL, 1 MBq) were prepared in 0.8 mL PBS and the solutions were incubated for 1 h in a shaking water bath at 37 °C. After 2 rounds of spinning and washing with PBS for 5 min at 1,500 x g, the decay corrected radioactivity of the pellet and supernatant was measured in a dose-calibrator. Following correction for background activity, the host-guest interaction was expressed as the percentage of the total amount of radioactivity (% binding).

    For stability measurements, either 0.1 mL MAA-Ad (0.1 mg/mL) with 0.1 mL ^{111}In-Cy$_{0.5}$CD$_9$PIBMA$_{39}$ (10 µg/mL, 1 MBq) or 0.1 mL ^{99m}Tc-MAA-Ad (0.1 mg/mL, 1 MBq) with 0.1 mL Cy$_{0.5}$CD$_9$PIBMA$_{39}$ (10 µg/mL) were prepared as described above and after removal of non-complexed materials the complex was diluted in either 0.8 mL PBS or FCS and incubated for 44 h in a shaking water bath at 37 °C. Following incubation durations of 2, 20, and 44 h, 0.1 mL samples were diluted in 1 mL of PBS and centrifuged for 5 min at 1,500 x g. The decay corrected radioactivity of both the pellet and supernatant was measured in a dose-calibrator. Hereby, the radioactivity of the pellet represented association of Cy$_{0.5}$CD$_9$PIBMA$_{39}$ to MAA-Ad (expressed as % of binding).

IMAGING EXPERIMENTS

Animals

In vivo studies were performed using 2–4-month-old Swiss mice (20-35 g, Crl:OF1 strain, Charles River Laboratories, USA). All animal studies were approved by the institutional Animal Ethics Committee (DEC permit 12160) of the Leiden University Medical Center. Mice were kept under specific pathogen-free conditions in the animal housing facility of the LUMC. Food and water were provided *ad libitum*.

Animal model

An embolization setup of the liver was performed according to previously described procedures.[15,17] In brief, [99mTc]-MAA-Ad (0.1 mg/mL, 2-5 MBq, n=6) was injected into the spleen of the mice (embolization step). Two h after embolization, a second injection with [111In]-Cy5$_{0.5}$CD$_9$PIBMA$_{39}$ (1 µg, 10 MBq) was administered I.V.. At 2, 12, 20, or 44 h the animals were imaged using SPECT and fluorescence imaging and quantified with biodistribution studies (see SPECT and fluorescence imaging protocols and biodistribution studies described below). Non-functionalized [99mTc]-MAA (0.1 mg/mL, 2-5 MBq, n=6), or mere PBS (n=3) served as controls.

General SPECT imaging

SPECT imaging was performed as previously described.[15] In brief, mice were placed and fixed onto a dedicated positioning bed of a three-headed U-SPECT-2 (MILabs, Utrecht, the Netherlands) at various intervals after injection of the host vector, while being under continuous 1-2% isoflurane anesthesia.[18] Radioactivity counts (range 0-600 keV) from total body scans were acquired for 30 min. For reconstruction from list mode data, the photo peak energy window was centered at 140 keV (for technetium-99m) or 240 keV (for indium-111) with a window width of 20%. Longitudinal differences in [111In] accumulation in mice were quantified by calculating radioactivity counts in regions of interest (ROI's). For this purpose, on the reconstructed images, using AMIDE's Medical Image Data Examiner (http://amide.sourceforge.net)ROI's were drawn over various tissues (including bone and joints as these were not assessed with routine biodistribution studies) allowing to determine radioactive counts in various tissues over time in a single mouse. ROI's drawn over the jugular veins were taken as a representative for the radioactivity in blood values. After imaging, mice were euthanized and the organs were removed and weighed to determine the percentage of injected dose per gram tissue (%ID/g). Blood samples obtained at various intervals of sacrifice, were used to determine the clearance from the blood fraction (expressed as the pharmacological half-life $t_{1/2}$) was calculated using GraphPad Prism version 5.01 for Windows (GraphPad Software, San Diego CA, USA).

Fluorescence imaging protocol

Dual-labeled Cy5$_{0.5}$CD$_9$PIBMA$_{39}$ was also equipped with a Cy5 fluorophore to perform confocal microscopy as described previously,[14,15] and in this study allows to perform macroscopic and eventually microscopic evaluation of the fluorescent signal of Cy5$_{0.5}$CD$_9$PIBMA$_{39}$ in excised tissues from mice using a preclinical IVIS Spectrum imaging

system (Caliper Life Science, Hopkinton, MA). Images of the Cy5-dye were acquired following excitation at 640 nm, and light was collected > 680 nm (acquisition time 5 s). Quantitative analysis of the fluorescence in the tissues (photons/sec/cm^2) was performed using the Living Image software from xenogeny v 3.2 (Caliper LS) at equal image adjustment settings.

Statistical analysis

All data are presented as mean value (±SD) of 3–6 independent measurements. Statistical analysis for differences between groups in the animal studies were performed by with Student's two-tailed independent samples T-test. Significance was assigned for *p*-values < 0.05. All analyses and calculations were performed using Microsoft® Office Excel 2010 and GraphPad Prism version 5.01 for Windows (GraphPad Software, San Diego, CA, USA).

RESULTS

Radiolabeling, functionalization, and stability of the vectors

Radiolabeling of guest vector with technetium-99m for 1 h at 37 °C yielded 92.8 ± 3.8% binding of the total added radioactivity. After incubating ^{99m}Tc-MAA in FCS at 37 °C for 20 h the release of radioactivity was shown to be less than 5%. Labeling of ^{111}In to Cy5$_{0.5}$CD$_9$PIBMA$_{39}$ for 1 h at 37 °C yielded 95.6 ± 3.6% of binding of the total added radioactivity determined by instant thin layer chromatography (ITLC). To determine the chelation stability, the host vector was incubated in FCS at 37 °C for 20 h. As depicted in Figure 1A the amount of ^{111}In-activity dissociating from the host after incubating in serum at 37 °C for 20 h was about 5% which indicates that the labeling was of the host with indium-111 was robust.

***In vitro* host-guest interactions**

Host–guest supramolecular interactions *in vitro* increased complexation of the ^{111}In-Cy5$_{0.5}$CD$_9$PIBMA$_{39}$ to MAA-Ad by nearly two-fold as compared to what was achieved with non-Ad-functionalized MAA (53.8 ± 4.3% vs 29.4 ± 5.1% respectively; *p*<0.001, n=8; Figure 1B). This indicates that host–guest interactions influence the complex formation. After 44 h incubation in either PBS or FCS, complex dissociation was found to be in the 10–20% range (see Figure 1C).
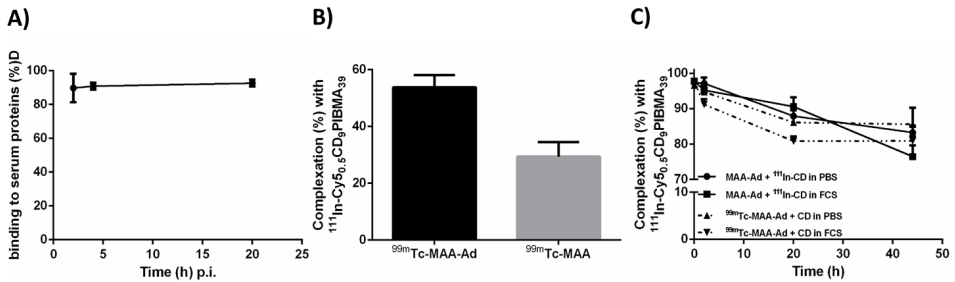
Figure 1. A) Serum binding of ^{111}In-Cy5$_{0.5}$CD$_9$PIBMA$_{39}$ over 20 h at 37 °C. **B)** *In vitro* host-guest complexation between guest vectors (MAA-Ad or MAA) and the host-vector (^{111}In-Cy5$_{0.5}$CD$_9$PIBMA$_{39}$) after 1 h at 37 °C. Data are expressed as the mean ± SD of the percentage of binding. **C)** *In vitro* stability determined at 37 °C of the host-guest complexation between guest vector MAA-Ad with host vector ^{111}In-Cy5$_{0.5}$CD$_9$PIBMA$_{39}$ in PBS or FCS (straight lines) and ^{99m}Tc-MAA-Ad with Cy5$_{0.5}$CD$_9$PIBMA$_{39}$ in PBS or FCS (interrupted lines). Values are expressed as the % of radioactivity associated with the washed pellet.

In vivo host-guest complex formation

To further validate the use of a supramolecular pre-targeting concepts during liver radioembolization, a non-tumor bearing animal model was used. The embolization setup in the liver was performed according to previously described procedures.[15,17] The most important reason for choosing this approach is that hepatic catherization in mice is invasive and would have resulted loss of many mice because of heavy bleedings. These bleeding would, in turn, have resulted in radioactive contaminations.

Dual-isotope SPECT imaging facilitated *in vivo* monitoring of host–guest interactions between ^{111}In-Cy5$_{0.5}$CD$_9$PIBMA$_{39}$ and ^{99m}Tc-MAA-Ad. The 6 h half-life of ^{99m}Tc meant its distribution could only be reliably monitored up to 20 h p.i. by means of SPECT imaging (Figure 2A). Biodistribution studies displayed residual ^{99m}Tc-MAA-Ad activity in the spleen (injection site; amounting to 80.4 ± 23.2%ID/g, 64.2 ± 5.6%ID/g, and 57.9 ± 8.4%ID/g at 2, 12, and 20 h p.i. respectively) and demonstrated prolonged diffusion of the radioactive signal from the spleen to the liver (amounting to 13.2 ± 2.2%ID/g, 36.4 ± 5.3%ID/g, and 43.0 ± 20.2%ID/g at 2, 12, and 20 h p.i., respectively; Figure S1).

Host–guest complexation between ^{111}In-Cy5$_{0.5}$CD$_9$PIBMA$_{39}$ and ^{99m}Tc-MAA-Ad was monitored *in vivo* by dual-isotope SPECT imaging. Figure 2B shows the distribution of the host vector in mice pretargeted with guest vector at 2, 12, 20 or 44 h p.i. of the host vector SPECT imaging of ^{111}In displayed the biodistribution of the host vector. As a result of the 2.8 d half-life of ^{111}In, the time-related uptake of the host vector in the liver of mice could
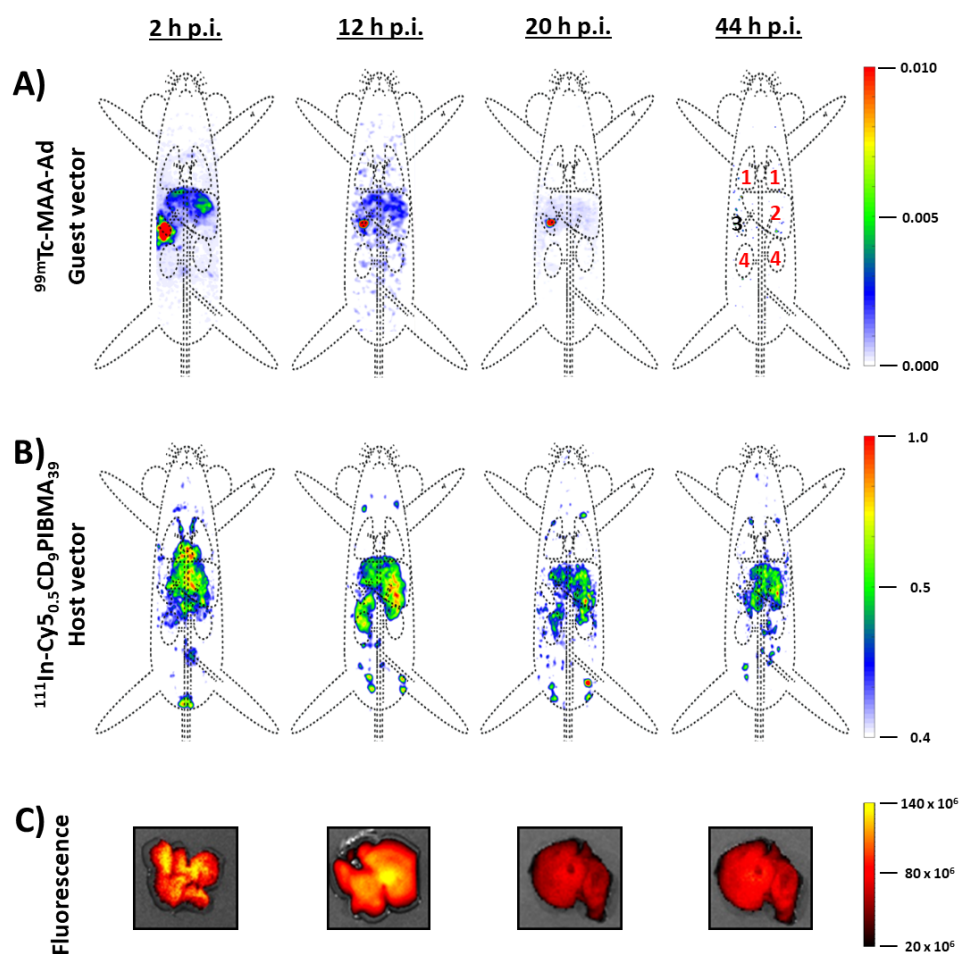
Figure 2. Time-related (2, 12, 20 and 44 h p.i.) dual-isotope SPECT biodistribution of **A**) intrasplenic administration of guest-vector ^{99m}Tc-MAA-Ad and **B**) Intravenous administered host-vector ^{111}In-Cy5$_{0.5}$CD$_9$PIBMA$_{39}$. Organs are marked as (**1**) lungs, (**2**) liver, (**3**) spleen, and (**4**) kidneys. The scale bars indicate the intensity of radioactivity expressed as arbitrary units. p.i. = post-injection.

be studied up to 44 h p.i. Longitudinal differences in ^{111}In accumulation were quantified either by calculating radioactivity counts in ROI's (Figure 4A–F) or as quantitative biodistribution studies (see Figure 5A & Table S1). These analyses revealed that at 20 h p.i. the hepatic uptake of the host vector was at its maximum (approximately 27 %ID/g). The observed intestinal uptake of ^{111}In-isotopes (Table S2) is indicative for hepatic uptake
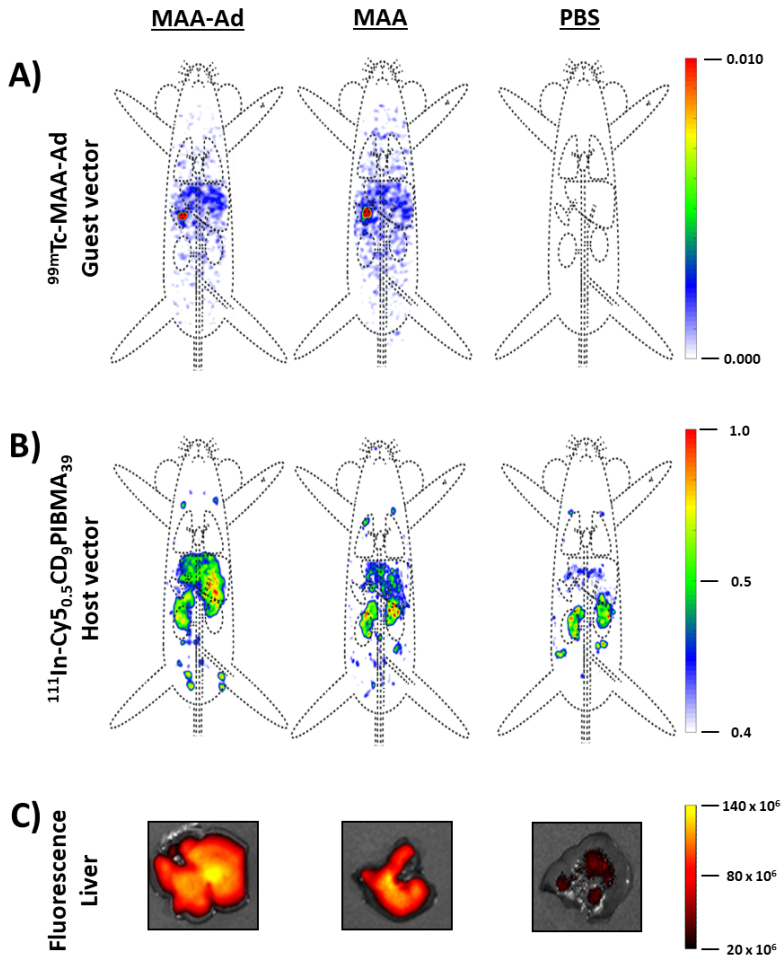
Figure 3. Dual-isotope SPECT biodistribution 12 h p.i. of **A)** mice pre-targeted with intrasplenic administration of guest vector ^{99m}Tc-MAA-Ad. Mice, pre-targeted with either non-functionalized ^{99m}Tc-MAA or PBS are used for comparison. Organs are marked as in Figure 2. **B)** Bio-distribution of host vector ^{111}In-Cy5$_{0.5}$CD$_9$PIBMA$_{39}$ after intravenous administration. **C)** Uptake of the host vector ^{111}In-Cy5$_{0.5}$CD$_9$PIBMA$_{39}$ in the liver determined by *ex-vivo* fluorescence imaging at equal settings. The scale bar indicates the intensity of fluorescence expresses as photons/sec/cm^2.

followed by intra-intestinal secretion. From 2 h onwards we observed small amounts of ^{111}In accumulation in the shoulder joints, knee joints, pelvis, kidney, and diffuse uptake in bone (Figure 2B, Figure 3B, Figure 4D), but bone uptake remained unchanged over time (Figure 2A, B, Figure 4D). Given the concurrence with known reservoirs for free ^{111}In^{3+},[19-21]
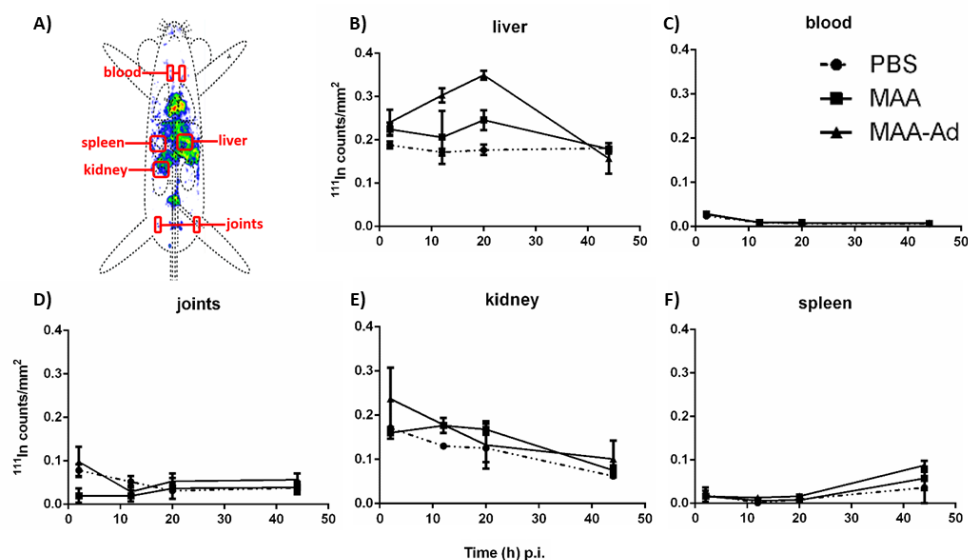
Figure 4. Time-dependent uptake of ^{111}In-Cy5$_{0.5}$CD$_9$PIBMA$_{39}$ in various tissues determined from **A)** radioactivity calculations in ROI's. Data are expressed as the ^{111}In radioactivity counts per mm^3 on the scintigrams in regions of interest (ROI's) drawn over **B)** liver, **C)** blood, **D)** joints, **E)** kidney, and **F)** spleen.

the isotope is most likely dissociated from the carboxylic acid moieties on the polymer backbone. Our results indicate that both methods, either by ROI's or biodistribution assays, provide an accurate representation of the accumulation of the host vector in various tissues in mice. Lung shunting, an essential property to prevent side effects due to off-target delivery,[2, 11] was not observed at any time point.

Liver uptake was increased by nearly 3-fold in mice treated with the functionalized pre-targeting vector ($p < 0.01$) as compared to the liver uptake of the host vector in control mice injected with ^{99m}Tc-MAA (10.8 ± 4.7 %ID) or PBS (8.6 ± 3.1 %ID; Figure 3B & Table S1, Figure 4B). Despite the presence of ^{99m}Tc-MAA(-Ad) signal in the spleen (see Figure 3A), accumulation of host vector in this organ was equal to that in PBS controls (Figure 4B & Table S1). Whether the hepatic uptake of the host vector in the animals that received ^{99m}Tc-MAA depended on non-specific interaction with MAA (as was measured *in vitro* Figure 1B) or because of the clogging of the microvasculature by MAA particles was undeterminable.
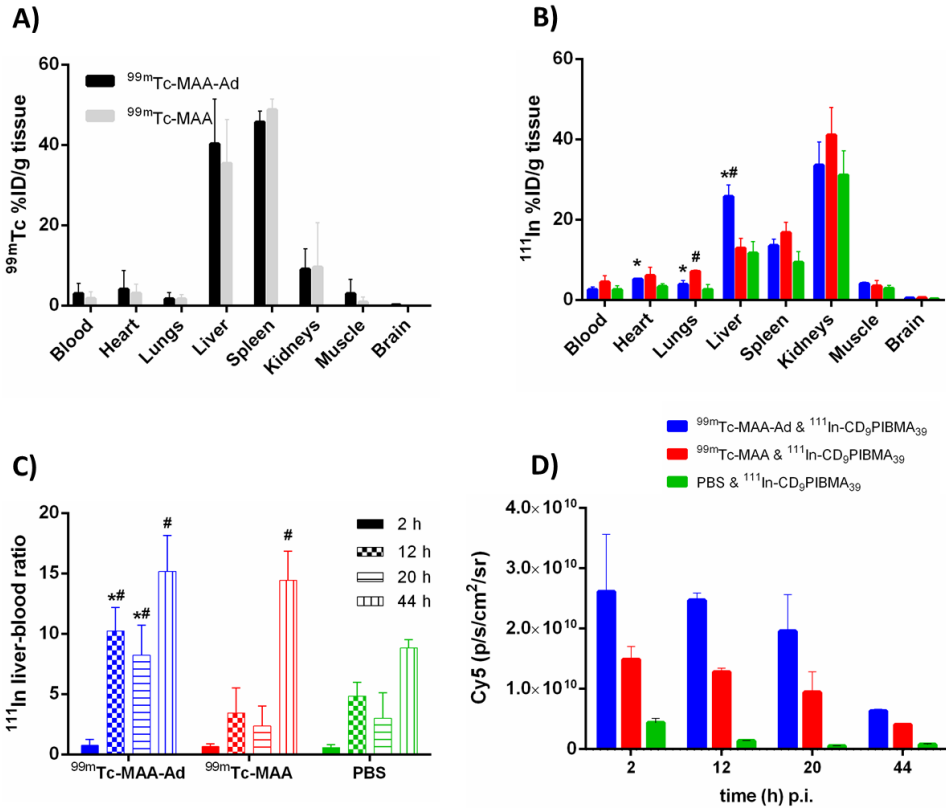
Figure 5. A) The bio-distribution of guest vectors ^{99m}Tc-MAA-Ad and ^{99m}Tc-MAA at various intervals after local administration. Data (expressed as the mean ± SD of the percentage of the injected dose per gram tissue (%ID/g) of 3 observations were calculated based on the radioactive counts measured in indicated tissues at 12, and 20 h post-injection. **B)** Biodistribution of intravenous administered ^{111}In-Cy5$_{0.5}$CD$_9$PIBMA$_{39}$ (host vector) 12 h after hepatic pre-targeting with guest vectors MAA-Ad (blue bars), MAA (red bars) or as control PBS (green bars). **C)** Dynamic hepatic uptake of intravenous administered host vector ^{111}In-Cy5$_{0.5}$CD$_9$PIBMA$_{39}$. Data are expressed as the mean ± SD ratios of the %ID/g in liver and blood measured at 2, 12, 20, and 44 h post-injection of the host vector. For all pre-targeting settings at 44 h p.i. liver-to-blood ratios for ^{111}In-Cy5$_{0.5}$CD$_9$PIBMA$_{39}$ are increased compared to the earlier intervals which is indicative for clearance of proteolytic or metabolic products. **D)** *Ex-vivo* fluorescence imaging analysis of the biodistribution of ^{111}In-Cy5$_{0.5}$CD$_9$PIBMA$_{39}$ in excised livers of mice pre-targeted with ^{99m}Tc-MAA-Ad, ^{99m}Tc-MAA, or PBS at various intervals until 44 h p.i. The fluorescence signal is determined from regions of interest (ROI's) drawn over the liver. Data are expressed as the average radiance p/s/cm^2/sr after correction for background activity. * = $p<0.01$ compared to ^{99m}Tc-MAA, #= p<0.01 compared to PBS.

Another interesting observation is the shorter blood half-life ($t_{1/2}$ = 192 min) calculated for the host vector in mice pre-targeted with guest vector ^{99m}Tc-MAA-Ad compared to the half-life of the host vector in mice pretargeted with control guest vector ^{99m}Tc-MAA ($t_{1/2}$ = 306 min) or PBS ($t_{1/2}$ = 318 min) (Table S2). The uptake of ^{111}In activity in other tissues, *e.g.*, blood, heart, lungs, muscle, and brains showed a decrease in uptake of ^{111}In radioactivity over time which was comparable between the two guest vectors or PBS (Table S1), most likely as a result of the clearance of ^{111}In-Cy5$_{0.5}$CD$_9$PIBMA$_{39}$ from these tissues. At all intervals liver-to-blood ratios for mice pre-targeted with ^{99m}Tc-MAA-Ad were highest whereby the liver-to-blood ratio peaked at 44 h p.i.

Fluorescence imaging

Ex vivo fluorescence imaging analysis of the biodistribution of the host vector in various excised tissues of mice pretargeted with guest vectors ^{99m}Tc-MAA-Ad and ^{99m}Tc-MAA revealed an intense fluorescence signal in the liver (Figure 3C & Figure 5D) at all time points after administration of the host (2.0–2.6 x 10^{10} p/s/cm^2/sr) which was highest for ^{99m}Tc-MAA-Ad compared to those for MAA (0.9–1.5 x 10^{10} p/s/cm^2/sr) or PBS (0.06–0.4 x 10^{10} p/s/cm^2/sr) which follows the trend as observed for radioactivity with ^{111}In-Cy5$_{0.5}$CD$_9$PIBMA$_{39}$. At 44 h p.i. all values dropped below 0.6 x 10^{10} p/s/cm^2/sr.

DISCUSSION

In this study we demonstrated that supramolecular interactions can form stable host–guest complexes between the host vector ^{111}In-Cy5$_{0.5}$CD$_9$PIBMA$_{39}$ and guest vector ^{99m}Tc-MAA-Ad *in vitro* and *in vivo*. The stability of these complexes over longer time periods strengthens the case for supramolecular pre-targeting strategies for radioembolization. Corroborating our previous results,[15] we did not observe lung shunting, an essential property to prevent side effects due to off-target delivery.[2,11] Since complex formation could be realized up until 20 h, the technology can accommodate single-session procedures whereby the host vector therapy is administered within hours after the scout scan (MAA-Ad; guest vector). In current clinical practice these procedures are performed several weeks apart.[22] A single-session procedure would be more patient-friendly as after the correct administration of the scout vector a therapeutic vector can be directly administered via the same catheter.[23] In addition to decreasing the invasiveness of the embolization procedure, cost reduction can also be achieved, as the secondary host vectors do not demand functionalization with

relatively expensive (*e.g.*, ^{90}Y or ^{166}Ho) isotopes, but could also act as carrier for cheaper therapeutical isotopes such as rhenium-188 or lutetium-177.[24] Uniquely for our approach is that isotope labelling could be converted into kit chemistry.

From SPECT images (Figure 2A, B, Figure 3A, B), biodistribution data (Figure 4, 5, Table S1), and fluorescence imaging (Figure 3C, Figure 5D) it may be concluded that, while initially predominantly present in the blood, ^{111}In-Cy5$_{0.5}$CD$_9$PIBMA$_{39}$ actively co-localizes with the MAA-Ad guest vector in the liver, resulting in increased uptake up to 20 h p.i. In addition to this conclusion, the 12 h timepoint gave the most optimal liver-to-blood ratios; Figure 2–4, Table S1). Clearly, the complex formation in the presence of MAA-Ad is unaffected by the strong serum interactions recorded for ^{111}In-Cy5$_{0.5}$CD$_9$PIBMA$_{39}$ (approximately 90%; Figure S1).

It was found that unbound host vector was excreted via both renal and hepatic clearance; most likely the latter occurred *via* the reticuloendothelial system.[25] The hepatic clearance complicates accurate performance assessments of hepatic and spleen signals at the 44 h time point. Ideally, future versions of the host vector are synthetically refined so that uptake in radiation-sensitive background organs such as the kidneys is minimized. This development may be achieved by dose optimization for the host vector or fine-tuning the polymer's functional groups[26]; these optimizations can possibly help to control the pharmacokinetics including the serum binding properties. In drug efficacy studies, it is often considered critical to account for plasma protein binding as this relates to the availability of the free drug, its half-life, and its subsequent renal elimination.[27] The lack of pulmonary shunting suggests ^{99m}Tc-MAA-Ad particles remained confined in the liver and are not released into the vasculature (Figure S1). Proteolytic breakdown of ^{99m}Tc-MAA-Ad as reported for pulmonary and hepatic injected ^{99m}Tc-MAA[28] was not observed in our experimental setup; no accumulation of unconjugated ^{99m}Tc-activity was observed in typical reservoir tissues, *e.g.*, thyroid, salivary glands and stomach.[19] This apparent increase in both MAA-Ad and MAA stability remains speculative, but we hypothesize that it could be attributed to a different proteolytic breakdown pathway of aggregated human albumin particles in mice.

We observed long-term complex formation, which was affected by only two small factors of dissociation. Firstly, dissociation of ^{111}In^{3+} from the host vector occurred in the initial phase after intravenous injection, which was in line with the 5% dissociation observed *in vitro*. The use of dedicated chelators that support stable chelation of the radioisotope could prevent this effect.[29] Secondly, *in vitro* for [^{111}In-Cy5$_{0.5}$CD$_9$PIBMA$_{39}$-^{99m}Tc-MAA-Ad] a 20% complex dissociation was observed over a 44 h timespan, which was confirmed *in*

vivo with the biodistribution assays. Indeed, a slow rate of excretion of about 20%/g for ^{111}In-Cy5$_{0.5}$CD$_9$PIBMA$_{39}$ was observed in this study. Again, future synthetic refinements could further address the stability by reducing the dissociation of the host vector and by improving the chelation of the radioisotope.

While serum–albumin binding is widely explored, clinical albumin-based nanodevices are more scarce.[30] Some examples are drug delivery of therapeutic agents with targeted albumin nanoparticles,[31] ^{99m}Tc-labeled albumin colloids for the visualization of the lymphatic vessels,[32] and surgical sentinel node detection with ICG-^{99m}Tc-nanocolloid.[33] With the presented radioembolization strategy we hope to promote the usage of biodegradable particles for nanomedicine.[34] Alternatively, the employed pre-targeting concept could be equally effective on different, *e.g.*, more spherical synthetic microparticles such as gold particles or quantum dots.[35-36]

A debate with regard to radioembolization technologies on whether or not the agents should be classified as medical technology or drugs is ongoing. Despite being chemical in nature and the fact that these agents administer a radiation dose to a patient even when used incorrectly, commercial microspheres are considered a medical device. Although the practical steps during the application are similar and the components don't actively interact with the body's metabolic or immune system (by relying on supramolecular interactions) may mean the proposed technology could be considered as a drug by the designated authorities. In that case it would affect the cost of translation and the quality standards that have to be met. The composition of the microparticles used as pre-targeting platform could potentially influence this selection.

CONCLUSIONS

The reported dual-isotope multiplexing and fluorescence imaging data further underlines the potential of using multivalent host–guest interactions between Ad and CD on albumin-based nanodevices *in vivo*. With that, a tool has been created that could help address unmet clinical needs in the field of radioembolization.

4

REFERENCES

1. A. Forner; J. M. Llovet; J. Bruix, Hepatocellular carcinoma. *The Lancet* **2012,** *379* (9822), 1245-1255.
2. F. E. Boas; L. Bodei; C. T. Sofocleous, Radioembolization of colorectal liver metastases: indications, technique, and outcomes. *J Nucl Med* **2017,** *58* (Supplement 2), 104S-111S.
3. G. A. van Hazel; V. Heinemann; N. K. Sharma, et al., SIRFLOX: randomized phase III trial comparing first-line mFOLFOX6 (plus or minus Bevacizumab) versus mFOLFOX6 (plus or minus Bevacizumab) plus selective internal radiation therapy in patients with metastatic colorectal cancer. *J Clin Oncol* **2016,** *34* (15), 1723-31.
4. H. S. Wasan; P. Gibbs; N. K. Sharma, et al., First-line selective internal radiotherapy plus chemotherapy versus chemotherapy alone in patients with liver metastases from colorectal cancer (FOXFIRE, SIRFLOX, and FOXFIRE-Global): a combined analysis of three multicentre, randomised, phase 3 trials. *Lancet Oncol* **2017,** *18* (9), 1159-1171.
5. D. Janevska; V. Chaloska-Ivanova; V. Janevski, Hepatocellular carcinoma: risk factors, diagnosis and treatment. *Open Access Maced J Med Sci* **2015,** *3* (4), 732-736.
6. R. Duran; J. Chapiro; R. E. Schernthaner, et al., Systematic review of catheter-based intra-arterial therapies in hepatocellular carcinoma: state of the art and future directions. *Br J Radiol* **2015,** *88* (1052), 20140564.
7. B. Sangro; L. Carpanese; R. Cianni, et al., Survival after yttrium-90 resin microsphere radioembolization of hepatocellular carcinoma across Barcelona clinic liver cancer stages: A European evaluation. *Hepatology* **2011,** *54* (3), 868-878.
8. R. Salem; R. J. Lewandowski; V. L. Gates, et al., Research reporting standards for radioembolization of hepatic malignancies. *J Vasc Intervent Radiol* **2011,** *22* (3), 265-278.
9. R. Hickey; R. J. Lewandowski; T. Prudhomme, et al., 90Y radioembolization of colorectal hepatic metastases using glass microspheres: safety and survival outcomes from a 531-patient multicenter study. *J Nucl Med* **2016,** *57* (5), 665-671.
10. L. Uliel, H.D. Royal, M.D. Darcy, et al., From the angio suite to the γ-camera: Vascular mapping and 99mTc-MAA hepatic perfusion imaging before liver radioembolization - A comprehensive pictorial review, *J Nucl Med* **2012** *53* (11) 1736-1747..
11. A. Riaz, R. Awais, R. Salem, Side effects of Yttrium-90 radioembolization, *Front Oncol* **2014**, *4* (198) 1-11.
12. M. Xing, S. Lahti, N. Kokabi, et al., 90Y Radioembolization lung shunt fraction in primary and metastatic liver cancer as a biomarker for survival, *Clin Nucl Med* **2016**, *41* (1) 21-27.

13. E. Garin, Y. Rolland, S. Laffont, et al., Clinical impact of (99m)Tc-MAA SPECT/CT-based dosimetry in the radioembolization of liver malignancies with (90)Y-loaded microspheres, *Eur J Nucl Med Mol I* **2016**, *43* (3) 559-75.

14. M. T. Rood; S. J. Spa; M. M. Welling, et al., Obtaining control of cell surface functionalizations via pre-targeting and supramolecular host guest interactions. *Sci Rep* **2017,** *7*, 39908.

15. S. J. Spa; M. M. Welling; M. N. van Oosterom, et al., A Supramolecular approach for liver radioembolization. *Theranostics* **2018,** *8* (9), 2377-2386.

16. M. Palmowski; A. Goedicke; A. Vogg, et al., Simultaneous dual-isotope SPECT/CT with ^{99m}Tc- and ^{111}In-labelled albumin microspheres in treatment planning for SIRT. *Eur Radiol* **2013,** *23* (11), 3062-3070.

17. H. Kasuya; D. K. Kuruppu; J. M. Donahue, et al., Mouse models of subcutaneous spleen reservoir for multiple portal venous injections to treat liver malignancies. *Cancer. Res.* **2005,** *65* (9), 3823-7.

18. M. M. Welling; A. Bunschoten; J. Kuil, et al., Development of a hybrid tracer for SPECT and optical imaging of bacterial infections. *Bioconjug Chem* **2015,** *26* (5), 839-849.

19. *Limits for intakes of radionuclides by workers*. Pergamon Press: Oxford, 1980; Vol. 4.

20. F. P. Castronovo, Jr.; H. N. Wagner, Jr., Comparative toxicity and pharmacodynamics of ionic indium chloride and hydrated indium oxide. *J Nucl Med* **1973,** *14* (9), 677-82.

21. E. H. Gilbert; J. D. Earle; E. Glatstein, et al., ^{111}indium bone marrow scintigraphy as an aid in selecting marrow biopsy sites for the evaluation of marrow elements in patients with lymphoma. *Cancer* **1976,** *38* (4), 1560-1567.

22. L. Sancho, M. Rodriguez-Fraile, J.I. Bilbao, et al., Is a technetium-99m macroaggregated albumin scan esential in the workup for selective internal radiation therapy with yttrium-90? An analysis of 532 patients, *J Vasc Intervent Radiol* **2017**, *28* (11) 1536-1542.

23. N. Rostambeigi, A.S. Dekarske, E.E. Austin, et al., Cost effectiveness of radioembolization compared with conventional transarterial chemoembolization for treatment of hepatocellular carcinoma, *J Vasc Intervent Radiol* **2014**, *25* (7) 1075-1084.

24. M.A. Lyra, A. Georgantzoglou, S. Kordolaimi, et al., Radioisotopes Production and Dosimetry, Nuclear Medicine Therapy, *Hellenic Association of Medical Physicists*, Athens, Greece, **2011**.

25. R. Lang; X. Jun-Hua; C. Bo, et al., Synthetic nanoparticles camouflaged with biomimetic erythrocyte membranes for reduced reticuloendothelial system uptake. *Nanotechnol* **2016,** *27* (8), 085106.

4

26. F. Alexis; E. Pridgen; L. K. Molnar, et al., Factors affecting the clearance and biodistribution of polymeric nanoparticles. *Mol Pharm* **2008,** *5* (4), 505-515.

27. D. A. J. Bow; J. L. Perry; J. D. Simon, et al., The impact of plasma protein binding on the renal transport of organic anions. *J Pharmacol Exp Ther* **2006,** *316* (1), 349-355.

28. O.S. Grosser, J. Ruf, D. Kupitz, et al., Pharmacokinetics of 99mTc-MAA- and 99mTc-HSA-Microspheres Used in Preradioembolization Dosimetry: Influence on the Liver-Lung Shunt, *J Nucl Med*, **2016**, *57* (6) 925-927.

29. R. Schibli; A. P. Schubiger, Current use and future potential of organometallic radiopharmaceuticals. *Eur J Nucl Med Mol Imag* **2002,** *29* (11), 1529-1542.

30. A. Loureiro; N. G. Azoia; A. C. Gomes, et al., Albumin-based nanodevices as drug carriers. *Curr Pharm Des* **2016,** *22* (10), 1371-90.

31. H. Kouchakzadeh; M. S. Safavi; S. A. Shojaosadati, Efficient delivery of therapeutic agents by using targeted albumin nanoparticles. *Adv Protein Chem Struct Biol* **2015,** *98*, 121-43.

32. N. S. Van den Berg; T. Buckle; G. I. Kleinjan, et al., Hybrid tracers for sentinel node biopsy. *Q J Nucl Med Mol Imaging* **2014,** *58* (2), 193-206.

33. G. H. KleinJan; E. van Werkhoven; N. S. van den Berg, et al., The best of both worlds: a hybrid approach for optimal pre- and intraoperative identification of sentinel lymph nodes. *Eur J Nucl Med Mol Imaging* **2018**.

34. M. Jamre; M. Shamsaei; M. Erfani, et al., Preparation and evaluation of [188]Re sulfide colloidal nanoparticles loaded biodegradable poly (L-lactic acid) microspheres for radioembolization therapy. *J Labelled Comp Radiopharm* **2018**.

35. M.-C. Daniel; D. Astruc, Gold nanoparticles: assembly, supramolecular chemistry, quantum-size-related properties, and applications toward biology, catalysis, and nanotechnology. *Chem Rev* **2004,** *104* (1), 293-346.

36. Y. Liu; H. Wang; Y. Chen, et al., Supramolecular aggregates constructed from gold nanoparticles and l-Try-CD polypseudorotaxanes as captors for fullerenes. *J Am Chem Soc* **2005,** *127* (2), 657-666.

SUPPORTING INFORMATION CHAPTER 4

In vivo stability of supramolecular host–guest complexes monitored by dual- isotope multiplexing in a pre-targeting model of experimental liver radioembolization

EXPERIMENTAL PROCEDURES

General

All chemicals were obtained from commercial sources and used without further purification. Solvents were obtained from Actu-All Chemicals (Oss, The Netherlands) in HPLC grade and used without further purification. The reactions were monitored by thin layer chromatography (TLC) and/or mass spectrometry using a Bruker microflex™ LRF MALDI-TOF. HPLC was performed on a Waters (Etten-Leur, The Netherlands) HPLC system using a 1525EF pump and a 2489 UV/VIS detector. For preparative HPLC a Dr. Maisch GmbH (Ammerbuch, Germany) Reprosil-Pur 120 C18-AQ 10 µm (250 × 20 mm) column was used (12 mL/min). For semi-preparative HPLC a Dr. Maisch GmbH Reprosil-Pur C18-AQ 10 µm (250 × 10 mm) column was used (5 mL/min). For analytical HPLC a Dr. Maisch GmbH Reprosil-Pur C18-AQ 5 µm (250 × 4.6 mm) column was used applying a gradient of 0.1% TFA in H_2O/CH_3CN 95:5 to 0.1% TFA in H_2O/CH_3CN 5:95 in 20 min (1 mL/min). NMR spectra were taken using a Bruker DPX-300 spectrometer (300 MHz 1H NMR, 75 MHz 13C NMR) and chemical shifts (δ) are reported relative to TMS (δ = 0) and/or referenced to the solvent in which they were measured.
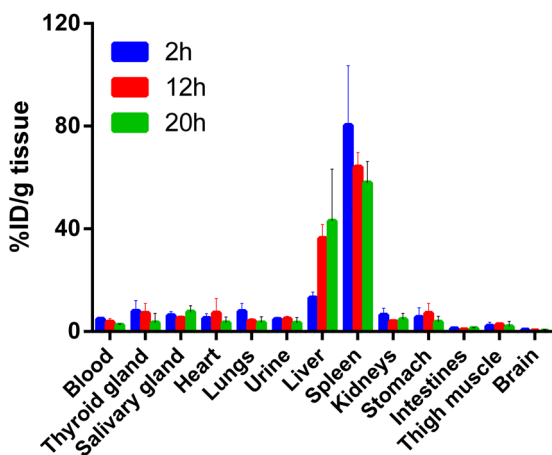

Figure S1. Quantified biodistribution of pre-targeting of the liver with locally administered primary vector (guest) ^{99m}Tc-MAA-Ad at various intervals. Data (expressed as the mean ± SD of the percentage of the injected dose per gram tissue (%ID/g) of 3 observations were calculated based on the radioactive counts measured in indicated tissues at 2, 12, and 20 h post-injection. Values of ^{99m}Tc-activity calculated at 44 h p.i. were deemed unreliable as the radioactivity counts were very low.

Table S1. The biodistribution of intravenously administered secondary vector (host) ^{111}In-Cy5$_{0.5}$CD$_9$PIBMA$_{39}$ (host molecule) after hepatic pre-targeting with guest molecules: ^{99m}Tc-MAA-Ad, ^{99m}Tc-MAA, or PBS. Data (expressed as the mean ± SD of the percentage of the injected dose per gram tissue (%ID/g) of 3-6 observations) were calculated based on the radioactive counts measured in various tissues at 2, 12, 20, and 44 h post-injection of the radioactive tracer. The significance of difference ($p<0.01$) is indicated with * compared to = ^{99m}Tc-MAA (control), or ‡ compared to PBS (^{111}In-Cy5$_{0.5}$CD$_9$PIBMA$_{39}$ reference distribution) according to Student's T-test.

Tissue	Time	Guest: ^{111}In-Cy5$_{0.5}$CD$_9$PIBMA$_{39}$		
	h p.i.	^{99m}Tc-MAA-Ad	^{99m}Tc-MAA	PBS
Blood	2	22.5 ± 6.4‡	18.1 ± 2.9‡	13.7 ± 1.9
	12	2.6 ± 0.6	4.4 ± 1.7	2.5 ± 1.0
	20	3.5 ± 0.8	3.8 ± 0.7	3.1 ± 1.3
	44	1.8 ± 0.2	1.6 ± 0.1	1.8 ± 0.3
Heart	2	10.2 ± 4.1*‡	8.0 ± 1.3	7.2 ± 1.5
	12	5.2 ± 0.2‡	6.0 ± 2.1	3.4 ± 0.6
	20	4.1 ± 0.3*	5.0 ± 0.9	3.9 ± 1.8
	44	8.3 ± 2.4‡	6.2 ± 0.6‡	4.5 ± 0.1
Lungs	2	10.2 ± 2.5*‡	7.6 ± 1.3	8.9 ± 1.4
	12	3.9 ± 1.0*	7.1 ± 0.4‡	2.6 ± 1.3
	20	4.2 ± 0.5*	5.3 ± 0.9	4.6 ± 1.8
	44	7.3 ± 1.1*	5.5 ± 1.3	7.6 ± 1.0
Liver	2	14.9 ± 6.1‡	11.4 ± 2.7‡	7.6 ± 2.3
	12	25.8 ± 2.9*‡	12.9 ± 2.5	11.7 ± 2.9
	20	27.0 ± 1.3*‡	10.8 ± 4.7	8.6 ± 3.1
	44	26.2 ± 2.1*‡	22.7 ± 2.3‡	15.7 ± 2.8
Spleen	2	9.7 ± 3.4‡	7.1 ± 0.8‡	5.5 ± 1.4
	12	13.5 ± 1.6	16.7 ± 2.6	9.4 ± 2.7
	20	11.8 ± 1.5‡	9.4 ± 0.5	10.2 ± 2.7
	44	17.9 ± 5.0*‡	13.0 ± 3.1	11.3 ± 0.7
Kidneys	2	20.9 ± 7.0*‡	10.0 ± 1.9‡	13.0 ± 2.3
	12	33.5 ± 5.8	41.1 ± 6.8	31.8 ± 6.1
	20	29.7 ± 5.3	29.2 ± 5.8	33.3 ± 12.2
	44	29.6 ± 3.6	29.7 ± 3.3‡	26.0 ± 3.6
Muscle	2	4.0 ± 1.9*‡	2.0 ± 0.4	2.2 ± 0.4
	12	4.0 ± 0.4	3.5 ± 1.4	2.9 ± 0.7
	20	2.2 ± 0.6*	3.4 ± 0.9	2.6 ± 0.6
	44	3.9 ± 0.4*‡	3.4 ± 0.3‡	3.6 ± 0.3
Brain	2	0.6 ± 0.2*‡	0.4 ± 0.1	0.4 ± 0.1
	12	0.4 ± 0.1‡	0.5 ± 0.2	0.3 ± 0.1
	20	0.3 ± 0.1	0.5 ± 0.2	0.3 ± 0.2
	44	0.5 ± 0.02‡	0.5 ± 0.04‡	0.4 ± 0.02

Table S2. The uptake of intravenously administered secondary vector (host) ^{111}In-Cy5$_{0.5}$CD$_9$PIBMA$_{39}$ in scavenging tissues, excretion rate and clearance. Data (expressed as the mean ± SD of the percentage of the injected dose per gram tissue (%ID/g) of 3-6 observations) were calculated based on the radioactive counts measured in various tissues at 2, 12, 20, and 44 h post-injection of the radioactive tracer. The significance of difference ($p < 0.01$) is indicated with *compared to = ^{99m}Tc-MAA (control), or ‡ compared to PBS (reference distribution) according to Student's T-test.

Tissue	Time	Guest		
	h p.i.	^{99m}Tc-MAA-Ad	^{99m}Tc-MAA	PBS
Urine & bladder	2	5.9 ± 0.8	6.2 ± 0.9	7.5 ± 1.5
	12	4.8 ± 1.7	4.3 ± 2.4	3.2 ± 0.6
	20	3.6 ± 0.9‡	4.7 ± 1.8‡	2.5 ± 0.6
	44	4.9 ± 0.7*	4.0 ± 0.7	5.6 ± 0.3
Thyroid gland	2	8.0 ± 2.9*‡	6.8 ± 1.7	5.8 ± 0.7
	12	8.2 ± 2.4	5.1 ± 5.2	5.3 ± 2.1
	20	6.2 ± 1.1	5.7 ± 2.1	5.8 ± 1.7
	44	6.0 ± 2.3	4.5 ± 2.2	5.8 ± 1.6
Salivary gland	2	5.8 ± 2.1*‡	4.3 ± 0.8	4.5 ± 0.8
	12	6.5 ± 1.3‡	7.6 ± 1.9	5.2 ± 1.1
	20	7.4 ± 0.7‡	7.5 ± 1.8	5.7 ± 1.5
	44	11.2 ± 0.4	11.3 ± 0.7	11.2 ± 4.6
Stomach	2	2.2 ± 0.9‡	1.9 ± 0.6	1.7 ± 0.6
	12	2.3 ± 0.7	1.5 ± 0.7	1.2 ± 0.9
	20	2.0 ± 1.0*‡	1.2 ± 0.8	0.9 ± 1.1
	44	5.6 ± 0.5‡	4.5 ± 0.8‡	6.7 ± 0.5
Intestines	2	5.1 ± 2.4*‡	3.2 ± 0.5	2.7 ± 0.6
	12	5.0 ± 2.8	8.1 ± 3.6	3.6 ± 1.5
	20	5.9 ± 0.7	8.4 ± 2.9	4.6 ± 3.0
	44	11.0 ± 1.8‡	7.7 ± 2.6	8.2 ± 0.5
Excretion (%ID)	2	4.5 ± 2.7	4.2 ± 6.1	3.6 ± 0.7
	12	11.1 ± 9.5‡	15.3 ± 9.3	21.0 ± 1.7
	20	14.3 ± 1.7*	8.5 ± 4.6	11.7 ± 3.6
	44	17.7 ± 2.4	18.8 ± 1.2	22.8 ± 5.0
Clearance		half-life t$_{1/2}$ (min)		
		192 (R2 0.864)	306 (R^2 0.980)	318 (R^2 0.943)

IN VIVO STABILITY OF HOST-GUEST COMPLEXES

Table S3. Dynamic hepatic uptake of intravenously administered secondary vector (host) ^{111}In-Cy5$_{0.5}$CD$_9$PIBMA$_{39}$. Data (expressed as the mean ± SD liver-to-blood ratios calculated between the percentages of the injected dose per gram tissue (%ID/g) of liver and blood (of 3-6 observations) based on the radioactive counts measured in these tissues at 2, 12, 20, and 44 h post-injection of secondary vector ^{111}In-Cy5$_{0.5}$CD$_9$PIBMA$_{39}$ after hepatic pre-targeting. The significance of difference ($p < 0.01$) is indicated with * compared to = ^{99m}Tc-MAA (control), or ‡ compared to PBS (reference distribution) according to Student's T-test.

Ratio	Time	Guest		
	h p.i.	^{99m}Tc-MAA-Ad	^{99m}Tc-MAA	PBS
Liver-to-blood	2	0.8 ± 0.5	0.7 ± 0.2	0.6 ± 0.2
	12	10.2 ± 2.0*	3.4 ± 2.1	4.9 ± 1.1
	20	8.2 ± 2.5‡	2.4 ± 1.6	3.0 ± 2.1
	44	15.2 ± 3.0‡	14.4 ± 2.4‡	8.8 ± 0.7

4